NJC

Accepted Manuscript

This is an *Accepted Manuscript*, which has been through the Royal Society of Chemistry peer review process and has been accepted for publication.

Accepted Manuscripts are published online shortly after acceptance, before technical editing, formatting and proof reading. Using this free service, authors can make their results available to the community, in citable form, before we publish the edited article. We will replace this *Accepted Manuscript* with the edited and formatted *Advance Article* as soon as it is available.

You can find more information about *Accepted Manuscripts* in the Information for Authors.

Please note that technical editing may introduce minor changes to the text and/or graphics, which may alter content. The journal's standard Terms & Conditions and the Ethical guidelines still apply. In no event shall the Royal Society of Chemistry be held responsible for any errors or omissions in this *Accepted Manuscript* or any consequences arising from the use of any information it contains.

ROYAL SOCIETY OF CHEMISTRY

www.rsc.org/njc

Ag_3PO_4 nanoparticle decorated on SiO_2 spheres for efficient visible light photocatalysis

Manu Sharma[a], Kasinath Ojha[a], Aparna Ganguly[b] and Ashok K. Ganguli[a,b,c*]

[a]Department of Chemistry, Indian Institute of Technology Delhi, Hauz Khas, New Delhi-110016, India.

[b]Nanoscale Research facility, Indian Institute of Technology Delhi, Hauz Khas, New Delhi-110016, India.

[c]Institute of Nano Science & Technology, Habitat Centre, Phase- X, Sector – 64, Mohali, Punjab–160062, India.

*Corresponding author: email: ashok@chemistry.iitd.ac.in; ashok@inst.ac.in phone- +91-11-2659-1511, fax: +91-172-2211074.

Abstract

Visible light active photocatalyst Ag_3PO_4 (20 nm) in combination with mesoporous SiO_2 sphere (200 nm) leads to enhanced photocatalytic activity (~ 52 times) in the photocatalytic degradation of Rhodamine B dye compared to bare silver phosphate. The lifetime of charge carriers is increased by nearly four times (from 0.05 to 0.20 ns) in the composite. The silver phosphate – silica composite has almost no loss of activity after 5 cycles under light irradiation indicating that the composite has good photocatalytic stability**.** The addition of SiO_2 also reduces the cost of the composite catalyst.

Introduction

Semiconductors are important for light harvesting and have excellent potential to offer solution to the existing environmental issues e.g. providing clean energy (water splitting), organic pollutants degradation, and CO_2 reduction. Surface property & band gap of a material typically affects the photocatalytic activity of the material which in turn is related to the composition and morphology of the said catalyst .[1–3] Other factors like surface energy of the exposed facet, high surface area and large optical absorption are some of the other key parameters which are operative for effective photocatalysis.[4] The exposed facets with higher surface energy can increase the number of catalytic active sites, which enhances the photocatalytic degradation of organic dyes.[5] Search for efficient visible light photocatalyst has engaged researchers for some time for water splitting and solar energy conversion.[6–8]

During the past few decades, several Ag-based semiconductor materials have been developed for photocatalytic water-splitting and the degradation of organics in wastewater.[9] Among other compounds of silver, Ag_3PO_4 is well known as a photosensitive material and has been extensively for the design of heterostructures with other semiconductors. Owing to its band gap and band potentials, silver phosphate exhibits extremely high photo-oxidative capabilities for O_2 evolution as well as organic dye decomposition under visible light irradiation.[10–12]

A breakthrough in the field of visible-light active photocatalysis was observed when Ye et al. reported a novel Ag_3PO_4 photocatalyst with high photo oxidative capability for water-splitting and organic dye degradation.[13] Apart from this, however, the stability of the

photo generated excitons is the most important factor for solar energy conversion. Low structural stability owing to its photo reduction & decomposition limits the practical usage of silver phosphate in its pure form. To overcome this, silver phosphate has been conjugated with several different classes of materials but majorly with semiconductors such as AgX/Ag_3PO_4 (X= Cl, Br, I),[14] Ag_3PO_4/TiO_2,[15] Fe_3O_4/Ag_3PO_4,[16] Ag_3PO_4/SnO_2,[17] Ag_3PO_4/CeO_2,[18] Ag_3PO_4/C_3N_4,[19,20] $Ag/Ag_3PO_4/TiO_2$,[21] $Ag_3PO_4/In(OH)_3$,[22] Ag_3PO_4/AgI,[23] CNT/Ag_3PO_4,[24] GO/Ag_3PO_4[25,26,27] and $Graphene/TiO_2/Ag_3PO_4$,[28,29] have been studied extensively as visible light photocatalysts with efficient activity. In Ag_3PO_4/TiO_2 composites, the stability of the Ag_3PO_4 is enhanced upon combining with TiO_2 as Ag^+ ions interact with O_2^- ions of TiO_2. Photogenerated charge transfer have been introduced by adding graphene in the composites.[27,28] A in-situ Z-scheme electron transfer was observed by introducing g-C_3N_4 in the composites.[20] The composites having higher dye adsorption capacity show higher efficiency and reusability of the photocatalyst.[16]

It is observed that the chemical stability of Ag_3PO_4 is enhanced in Ag_3PO_4/SnO_2, composite under visible light irradiation and shows enhanced degradation of methyl orange dye owing to the ease of separation and transport of photo-generated electrons and holes in the composite material leading to the enhancement of photocatalytic efficiency.[18] Various solid supports like polymers, carbon materials and metal oxides have been used in the designing of composite photocatalyst to improve the catalytic activity and stability of the material.[30–34] Recently, Yan et al have reported Ag_3PO_4 (diameter ~200 nm) loaded SiO_2 microspheres with efficient methyl orange degradation on visible light irradiation[35].

Generally development of photocatalytic system includes two parts. First being the designing & synthesis of nano sized photocatalyst and the second being to engineer a

photocatalytic system creating large active area and facilitating effective mass transfer during the course of reaction. Thus, in this study, we have chosen, SiO_2 nanoparticles as a catalyst support owing to its high chemical inertia, thermal stability, large specific surface area and high absorption that facilitates the interfacial reaction of the composite material. A recent report shows enhanced photocatalytic degradation of methyl orange using silver phosphate (~200 nm) in a composite with large SiO_2 spheres (~800 nm) while bare silver phosphate shows better photocatalytic degradation of Rhodamine B (RhB) than the composite with SiO_2.[35] Here have shown much better photocatalytic performances of the composite for RhB degradation in comparison to bare silver phosphate. We have used smaller Ag_3PO_4 (~20 nm) particles decorated on SiO_2 (~200 nm) spheres where enhanced lifetime of the photo-excited electron of silver phosphate in the composite leads to remarkable enhancement (~52 times) in the photocatalytic activity. We have also looked into the mechanism followed for the degradation process in detail.

Experimental

Materials

All the chemicals were of analytical grade and have been used without any further purification. Silver nitrate (Sigma Aldrich), disodium hydrogen phosphate (Fisher scientific), cetyltrimethyl ammonium bromide (CTAB) (Spectrochem Laboratories), ethanol (Merck) and ammonia solution (Fisher scientific) were used. The solutions were prepared in double distilled water.

Synthesis of silver phosphate decorated silica spheres

Silver phosphate decorated silica spheres were synthesized using co-precipitation method at room temperature. For the synthesis of nanocomposites, first the silica spheres were synthesized using hydrothermal method in presence of surfactant. 0.50 g of CTAB and 1 M of tetraethylorthosilicate (0.25 mL) were added in a mixture of water (7 mL) and ethanol (6.3 mL).[36] Ammonia solution (0.5 mL of 25 %) was added dropwise to the mixture and stirred for 15 min. The mixture was then loaded in a 100 mL hydrothermal bomb with Teflon lining and heated at 120° C for 48 h. The product was collected by centrifugation followed by washing with water, the precursor was dried at 70° C and further heated in a furnace at 550 °C for 5 h to remove the CTAB surfactant or organic moiety from the silica spheres.[37] The composite materials have been synthesized at three different weight ratio of 1:2.8 (SA1), 1:8.4 (SA2) and 1:16.8 (SA3) of silica and silver phosphate. In the synthesis of SiO_2-Ag_3PO_4 composite, first SiO_2 powder (50 mg) was sonicated in water then an aqueous solution of silver nitrate was added and finally disodium hydrogen phosphate was added dropwise into the suspension. Silver nitrate (0.170g, 0.50g and 0.10 g in 50 mL water) and disodium hydrogen phosphate (0.048, 0.144 and 0.288 g in 50 mL water) were taken for the synthesis of composites SA1, SA2 and SA3 respectively. After the addition of disodium hydrogen phosphate a yellow color product was formed. This yellow color precipitate was centrifuged, washed and dried at 70°C. Nomenclature and concentration of different silver decorated silica spheres are summarized in Table S1.

Characterization

Powder X-ray diffraction (XRD) studies were carried out on a Bruker D8-Advance powder X-ray diffractometer with Cu-Kα radiation (λ = 1.5418 Å). FTIR spectroscopy

studies (using KBr disks) were carried out using a Nicolet Protege 460 Fourier transform infrared (FTIR) spectrometer in the range of 400-4000 cm^{-1}. Transmission electron microscopy (TEM) and energy dispersive X-ray analysis studies were carried out using FEI Technai G2 20 electron microscope operating at an accelerating voltage of 200 kV. For recording the diffuse reflectance spectra of the solid samples, UV-Visible spectrophotometer Shimadzu UV-2450, was operated in solid state mode in wavelength range of 250–800 nm with barium sulphate as the reference. Nitrogen adsorption–desorption isotherms were recorded at liquid nitrogen temperature (77 K) using a Nova 2000e (Quantachrome Corp.) equipment and the specific area was determined by the Brunauer–Emmett–Teller (BET) method. The samples were degassed at 150 ºC for 12 h prior to the surface area measurements. The photoluminescence spectra of the samples were recorded by dispersing the sample in ethanol and with excitation at 370 nm. Time-resolved photoluminescence was carried out on Edinburgh instrument (FLS980 Fluorescence Spectrometer) with the excitation at 377 nm. The data obtained from the lifetime studies was analysed with the aid of the software (decay fitting).

For the photocatalytic degradation of Rhodamine B, 50 mg of the catalyst was dissolved in 50 ml of 12 μM Rhodamine B dye solution and the mixture was irradiated with visible light using a tungsten lamp (100 W). Adsorption capacity of the material was checked by allowing the sample to equilibrate in the dye solution for 30 mins under dark conditions. After 30 minutes of stirring in dark the visible light source was switched on. The photodegradation of Rhodamine B dye in aqueous solution was monitored using the absorption maxima at 546 nm.

Electrochemical impedance spectroscopy measurements were carried out using Metrohm Auto lab 302/PGSTAT. The composite materials (2 mg) were dispersed homogeneously in 10 µL of the mixture of isopropanol and Nafion (1:1). Then 5 µL of the mixture were placed on glassy carbon electrodes (0.03 cm^2) followed by drying on air. The composite coated glassy carbon electrode was used as working electrode with Ag/AgCl as reference electrode and Pt wire as counter electrode. 0.1M Na_2SO_4 aqueous solution was used as electrolyte. The measurement was carried out at 0.4V vs. Ag/AgCl with an amplitude of 10 mV in the frequency range of 100 kHz - 0.1 Hz.

Results and discussion

Characterization of silver phosphate decorated silica spheres:

Pure silver phosphate (A) and the composite material (SA1) were characterized using powder x-ray diffraction. Fig.1a confirms the formation of pure cubic phase of silver phosphate (JCPDS NO. 84-0512), while Fig.1b confirms the presence of silver phosphate in the composite.

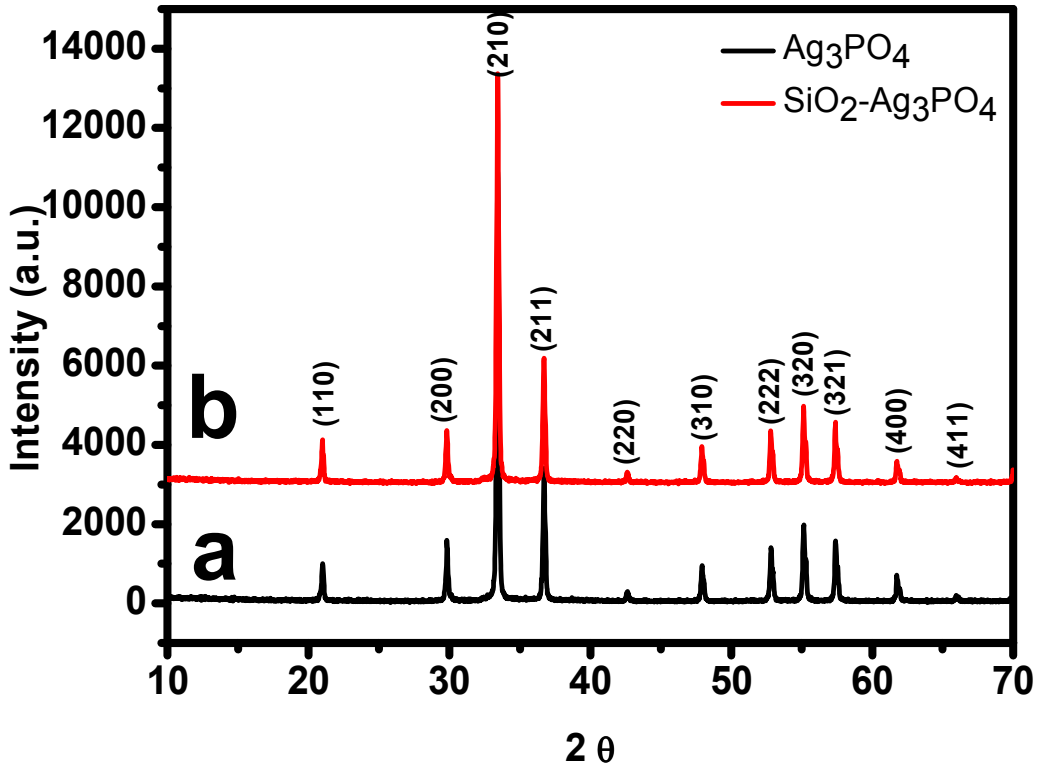

Fig. 1. PXRD pattern of (a) Ag_3PO_4 and (b) SiO_2-Ag_3PO_4 (SA3).

Since silica is amorphous, its presence in the composite was confirmed by the presence of Si-O, Si-O-Si, Si-OH vibrational bands in the IR spectra of the composite.[36] The band observed at 1427-1429 cm^{-1} due to H-O-H bending. The two strong bands observed at 1017 and 560 cm^{-1} can be attributed to molecular vibration of phosphate ions (P-O stretching).[9,21] The band observed at ~ 3454 to 3336 cm^{-1} is due to –OH stretching. The IR bands have been tabulated in Table S2.

TEM image of pure silver phosphate nanoparticles (A) shows agglomerated spherical particles of ~20 nm (Fig. 2). The TEM studies of the composites show ~20 nm nanoparticles embedded on ~200 nm spheres (Fig. 2). The larger spheres are presumably

of silica as bare SiO_2 spheres (~200-500 nm diameter) was observed in TEM micrograph (Fig. S1). From the TEM images, it is observed that the sample obtained at lower molar ratio (SA1), a small number of silver phosphate particles were present on the surface of silica spheres.

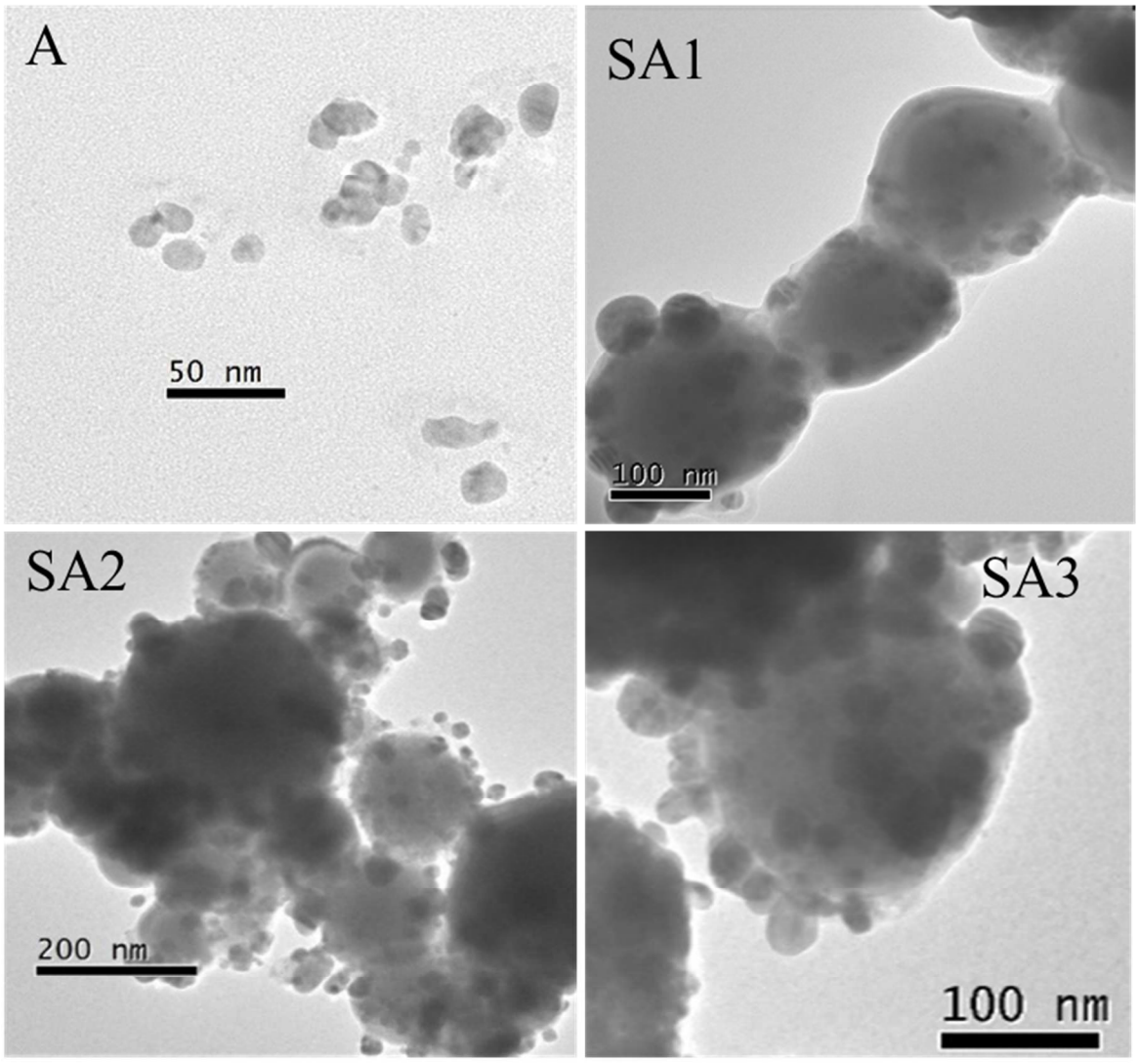

Fig. 2. TEM images of A, SA1, SA2 and SA3 samples obtained using different ratios of silica and silver phosphate.

When the concentration of silver and phosphate ions increases (SA2, SA3) more number of Ag_3PO_4 particles were observed on silica surface (Fig. 2). Crystal planes corresponding to cubic Ag_3PO_4 have been observed in HRTEM of SA3 (Fig. 3a) where (200), (211) and

(210) planes could be indexed. Electron diffraction of Ag_3PO_4 particles (Fig. 3b) shows the bright spots correspond to the cubic Ag_3PO_4 phase (Fig. 3d), however there are random spots due to multiple crystals. Energy dispersive X-ray analysis (EDAX) data of SA3 sample shown in Fig.S2 confirms the presence of Si, P, O and Ag without any other impurities. Elemental mapping in SEM micrograph clearly shows the presence of the elements (Fig. 3c-h). The optical properties and the band gap of A, SA1, SA2 and SA3 samples were studied using diffuse reflectance spectroscopy (DRS) in the range of 250 to 800 nm. Diffuse reflectance spectra of pure silver phosphate (A) and composite material (SA3) has been shown in Fig. S3.

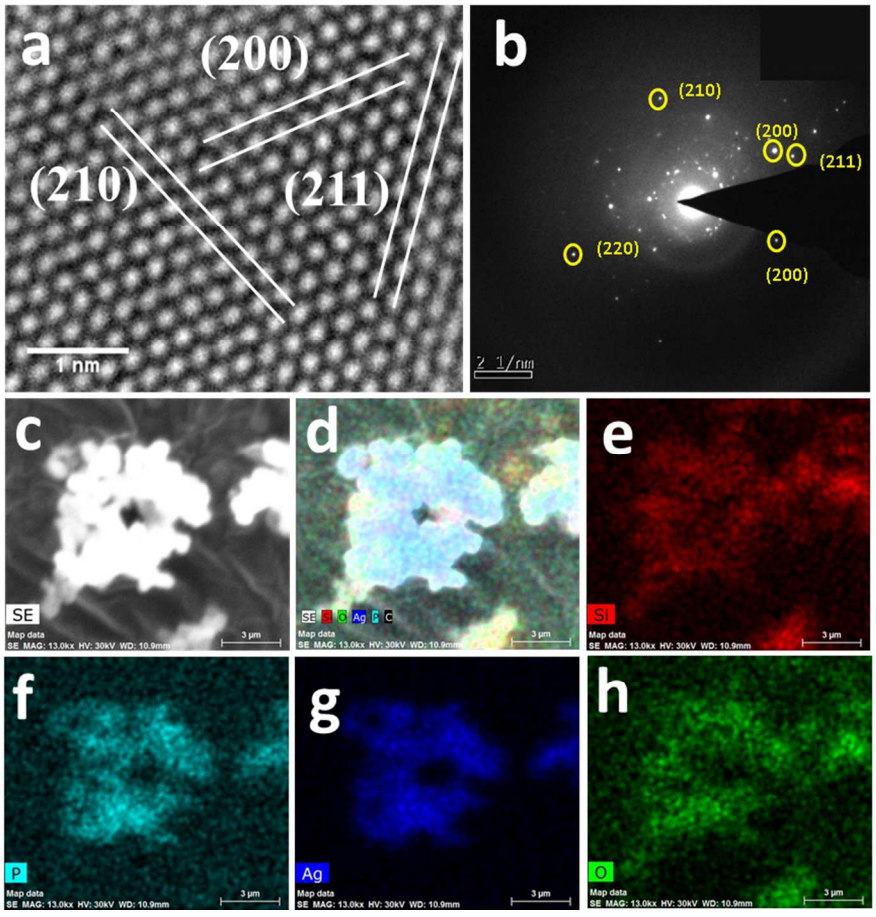

Fig. 3. High resolution TEM image (a) SA3 samples, (b) electron diffraction pattern of SA3 and indexed with (211), (200), (220), and (210) lattice fringes. (c-h) SEM elemental mapping showing different elements present in SA3 composite.

The band gap for all the compositions were evaluated with the help of Kubelka-Munk equation. We observe a blue shift in the absorption edge on increasing the concentration of silver phosphate in the composite i.e. from 502 nm to 478 and 473 nm. Pure silver phosphate shows band gap of ~ 2.47 eV which increases to 2.62 eV when it's conjugated with silica in the composite. The photoluminescence spectra of A and SA3 samples was recorded under excitation at 375 nm. In the photoluminescence spectra, the peak observed at 430 nm arises due to intrinsic states rather than the surface states.[22] The emission peaks observed at 483 and 528 nm are attributed to oxygen vacancies in silver phosphate (Fig. S3).[38,39] As the concentration of silver phosphate nanoparticles is increased the band gap of the composite decreases from 2.62 eV (SA1) to 2.59 eV (SA3). The surface area, pore size and pore volume of pure silver phosphate (A) and silver phosphate decorated silica spheres (SA1, SA2, SA3) have been tabulated in Table 1.

Table 1. BET surface area, pore size and pore volume of A, SA1, SA2 and SA3 samples with varying concentration of silver phosphate.

Sample	BET surface area (m2 /g)	Pore size (nm)	Pore volume (cc/g)
SiO_2	86	15	0.16
A	20	36.5	0.030
SA1	42	21.3	0.070
SA2	43	24.3	0.068
SA3	45	27.2	0.060

The adsorption-desorption plot of pure silver phosphate (A) and silver phosphate decorated silica spheres (SA3) shows the type-IV adsorption isotherm (Fig. 4). The surface area of pure silver phosphate (A) was found to be 20 m^2/g whereas for the

composite it was ~ 40 m^2/g. The enhancement in surface area of composite material in presence of silica support is mainly due to the presence of mesoporous silica spheres. There is no change in the specific surface area of the composites with increase in the concentration of silver phosphate.

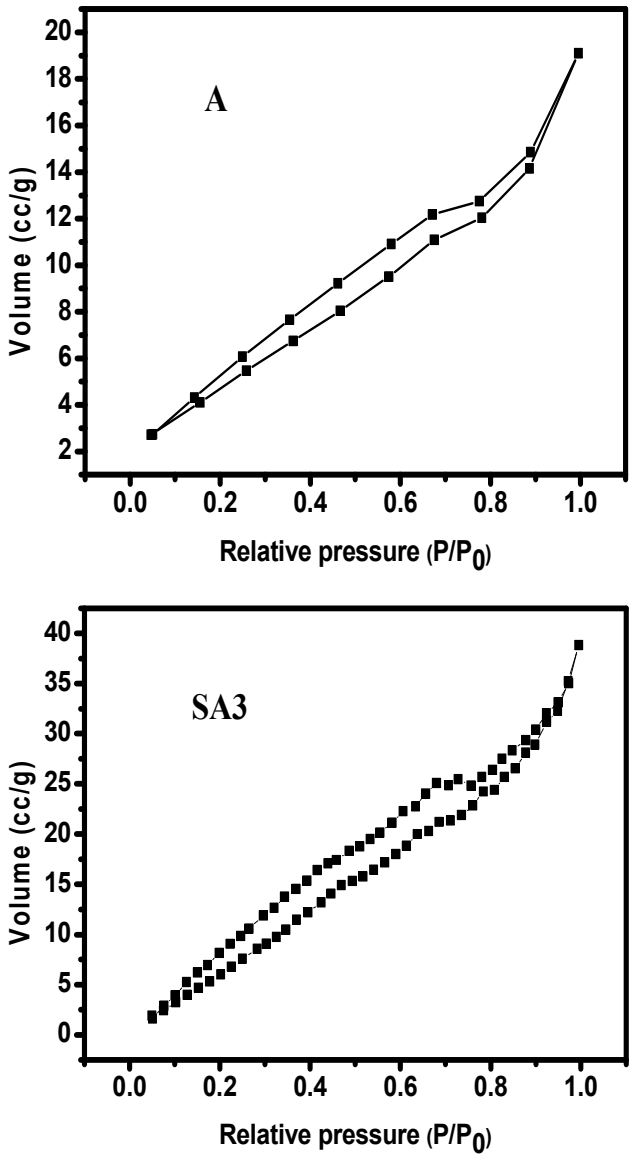

Fig. 4. Adsorption-desorption plot of pure silver phosphate (A) and silver phosphate decorated silica spheres (SA3).

Photocatalytic activity of silver phosphate decorated silica spheres:

To check the photocatalytic activity of the catalyst, the degradation of Rhodamine B dye under visible light irradiation was studied (Fig.5). No catalytic degradation of RhB was observed in dark in presence of the composites. Three different samples with varying compositions of silver phosphate (SA1, SA2 and SA3) have been used as the photocatalyst for Rhodamine B degradation. The dye degradation rate was found to increase with increase in the concentration of silver phosphate (the number of interfaces between silver phosphate and silica increased with conc. which enhances the catalytic activity by delaying the recombination rate). Thus, the overall degradation depends on the silica support as well as on the concentration of silver phosphate.

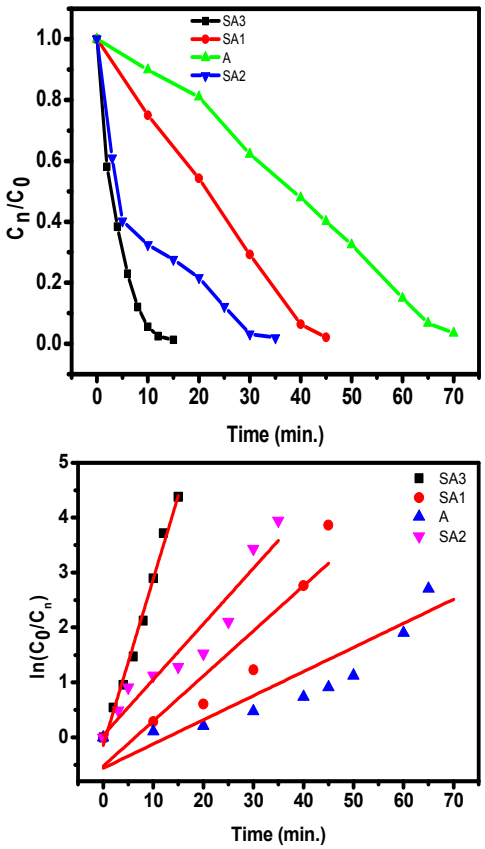

Fig. 5. Photodegradation of Rhodamine B dye using pure silver phosphate (A) and silver phosphate decorated silica spheres (SA1, SA2 and SA3) under visible light irradiation.

Photocatalytic reaction follows pseudo unimolecular kinetics, rate constant and half-life of the reactions that have been tabulated in Table 2. The maximum rate (0.26 min^{-1}) was observed in case of SA3 where the concentration of Ag_3PO_4 is highest (Table 2).

Table 2. Rate constant, half-life and band gap of A, SA1, SA2 and SA3 samples with varying the concentration of silver phosphate.

Sample	Rate constant (min^{-1})	% error	$t_{1/2}$ (min)	Band gap (eV)
A	0.0050	14	138.6	2.47
SA1	0.0062	29	111.8	2.62
SA2	0.15	5	4.62	2.60
SA3	0.26	1	2.67	2.59

The photocatalytic decomposition of rate of composite material (SA3) is approximately 52 times higher than pure silver phosphate (A). On the other hand the degradation rate of SA1 and SA2 samples was found to be 0.0062 min^{-1} and 0.15 min^{-1} respectively. However, we observed very low photocatalytic activity similar to pure silver phosphate (Fig.S5) when we further increased the amount of silver phosphate in the composite (weight ratio 1:33.6).

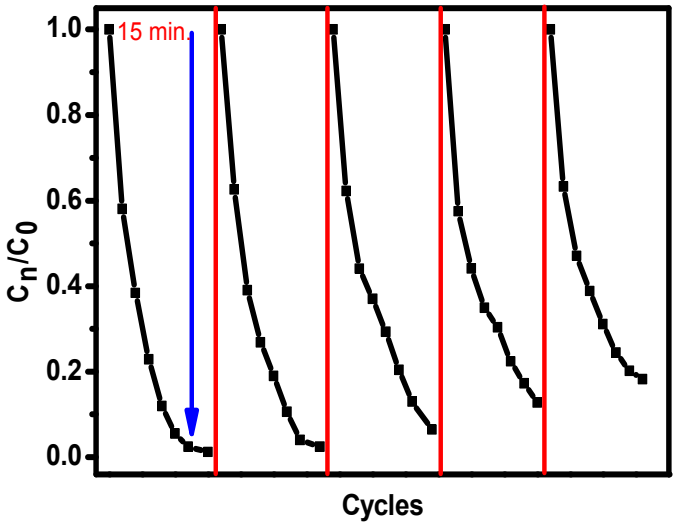

Fig. 6. Recyclability of silver phosphate decorated silica spheres (SA3) under visible light irradiation for 15 minutes.

The photo activity of the catalyst was found to increase with increase in the surface area. The large surface area can promote the high catalytic activity because more and more sites are available for dye molecules to be adsorbed on the catalyst. The reusability of the photocatalyst SA3 has been determined for five consecutive cycles (Fig. 6) and it was found that the catalyst was highly stable. The role of the SiO_2 spheres is to increase the crystallinity of Ag_3PO_4 and high dye adsorption in the vicinity of Ag_3PO_4 particles leading to reduction of the self-recombination of Ag_3PO_4 excitons. There are reports on the interplay of Lewis acidity of SiO_2 and the interface between SiO_2 and semiconductor on enhancement of photocatalytic activity.[40] In the composites, surface functionalities like Si-OH bonds help in promotion of O_2 adsorption which favours the separation of the photogenerated charge carriers.[41] More number of interfaces between two materials and formation of new surface states in the composites traps electrons/holes which increases the charge separation resulting enhancement in the overall lifetime of the photo-excited electrons.[42] We have shown that the photocatalytic activity of composite increases with the

increase of silver phosphate. However, further increase in the amount of Ag_3PO_4, the contribution from SiO_2 will be negligible (as shown by our experiments which we have added in the supplementary document, Fig.S5).

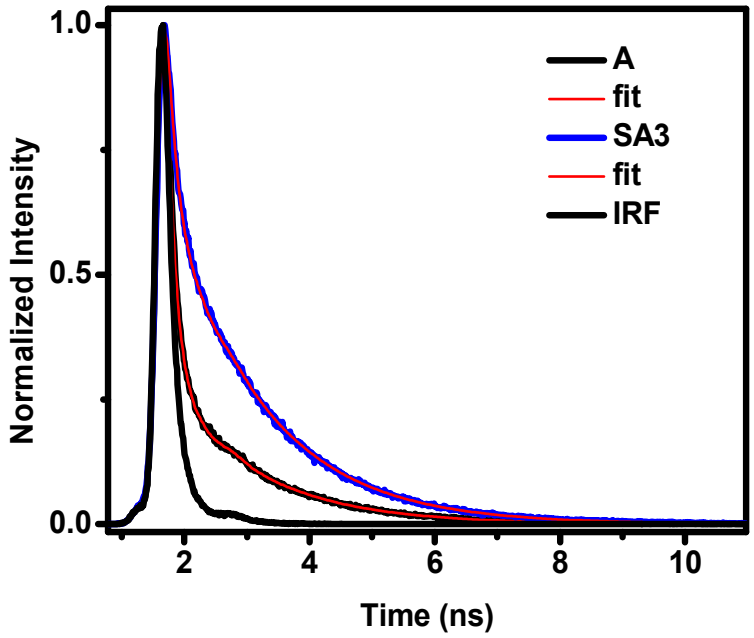

Fig. 7. Time-resolved photoluminescence of pure Ag3PO4 (A) and silver phosphate decorated silica spheres (SA3).

Steady State photoluminescence studies shows emission bands at 430 nm, 483 nm and 528 nm (Fig. S4) for Ag_3PO_4. To study the delay in the exciton recombination we have carried out time-resolved photoluminescence studies with excitation at 377 nm. The lifetime of the excited electrons increased from 0.05 to 0.20 ns in the hybrid materials in comparison to bare Ag_3PO_4 (Fig. 7). Photo-generated electron may transfer from the Ag_3PO_4 to O_2 adsorbed on SiO_2 surface at the interface between SiO_2 and Ag_3PO_4 leading to longer lifetime of the electron which is evident from the lifetime data (Table S3). Nyquist (-Z'' vs. Z') plot of pure Ag_3PO_4 (A) and composites (SA1, SA2, SA3) at zero applied bias has been shown in Fig. 8.

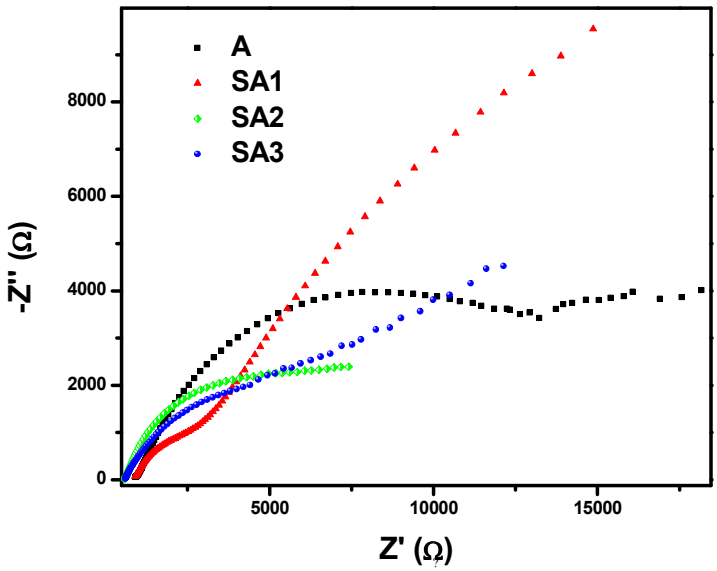

Fig. 8. Nyquist (-Z'' Vs Z') plot of pure Ag3PO4 (A) and composites (SA1, SA2, SA3).

The diameter of the semicircle on the Nyquist plot of the composites are much smaller than that of pure Ag_3PO_4 (A). This indicates lower charge transfer resistance of the composite than bare silver phosphate. The composite material with higher silver phosphate (SA3) shows much lower charge transfer resistance than bare Ag_3PO_4. This may be due to the surface functionalities (Si-OH) and trapping sites which enhances the charge separation.

Mechanism:

To understand the mechanism followed by silver phosphate decorated silica spheres towards the photocatalytic dye degradation, several experiments were carried out.

The schematic diagram for the proposed mechanism of silver phosphate decorated silica spheres under visible light irradiation has been shown in Fig. 9. During a photocatalytic reaction, electrons & holes are generated under visible light irradiation.

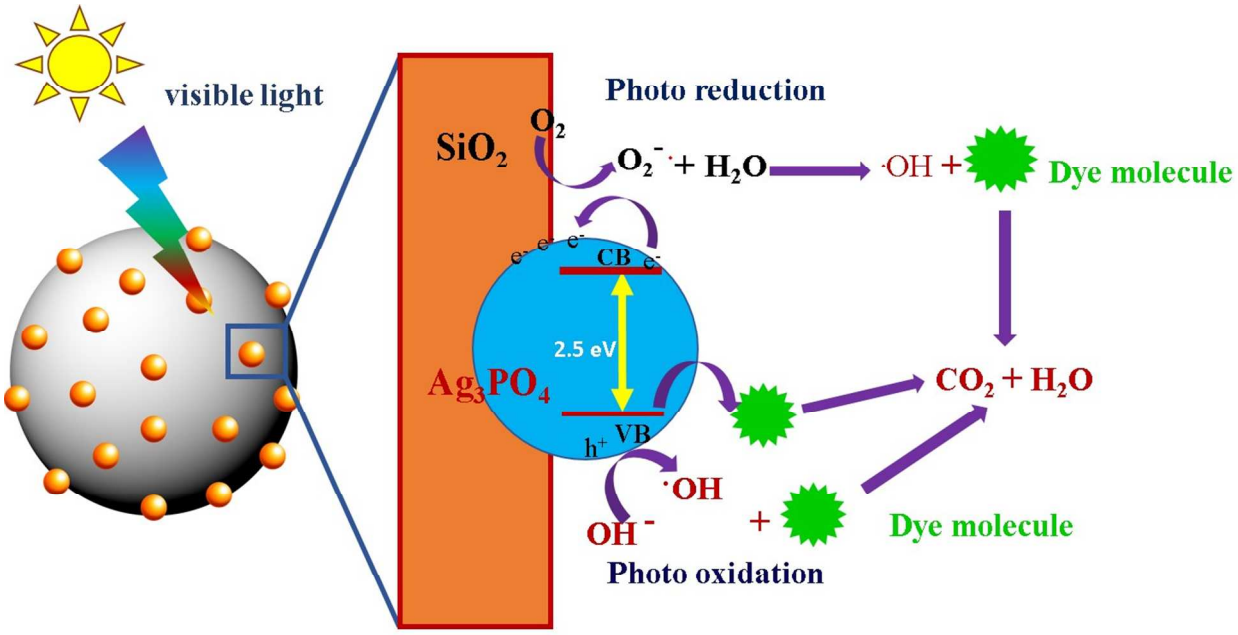

Fig. 9. Schematic diagram for the dye degradation mechanism followed by the silver phosphate decorated silica spheres under visible light irradiation using Rhodamine B dye.

It is assumed that the photogenerated electrons in conduction band of silver phosphate move to the interface between silver phosphate and SiO_2 particle. The interface trapped electrons supposedly react with the dissolved oxygen molecules and generate superoxide radical anions $O_2^{\bullet -}$. The superoxide radical anions react with water molecules and generate the hydroperoxy radicals ($HO_2^{\bullet}$) and finally produce hydroxyl radicals ($OH^{\bullet}$). The holes (h^+) in valence band are trapped by surface hydroxyl groups or H_2O at the catalyst surface to yield $OH^{\bullet}$. The hydroxyl radicals are very strong oxidizing agent which assist in the decomposition of the organic dye molecules. To understand the role of the excited electrons and the holes in the degradation mechanism (RhB), different types of scavengers have been used. (Fig. 10). The effect of isopropyl alcohol, EDTA and benzoquinone as hydroxyl radical scavenger, hole scavenger, and superoxide radical scavenger respectively have been studied here.[43]

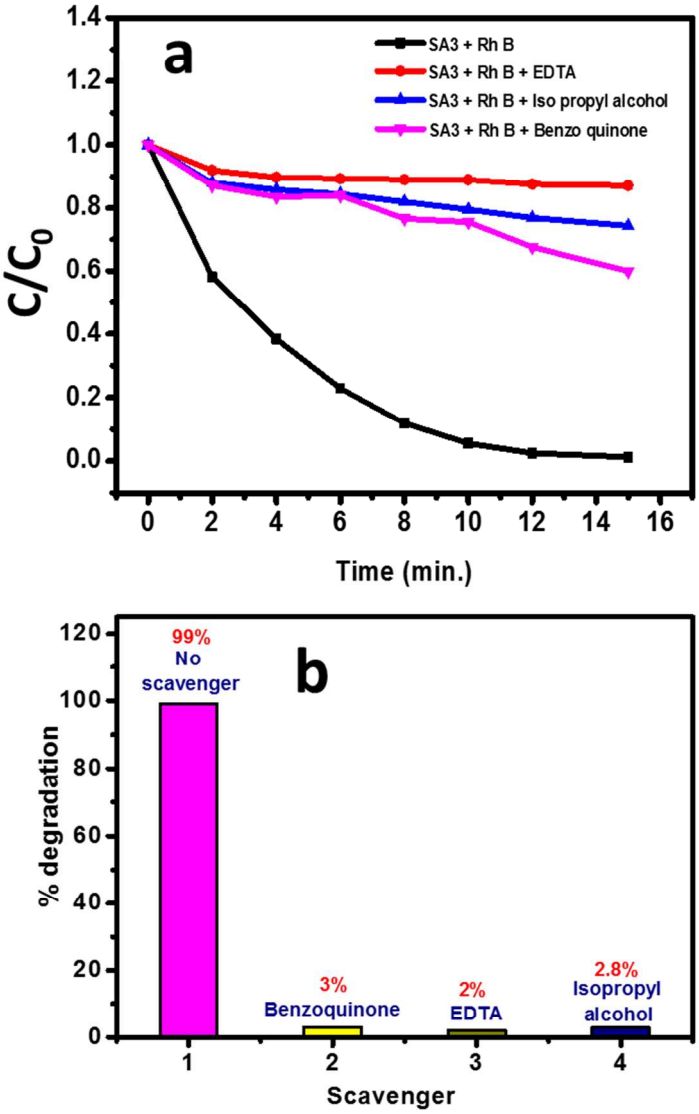

Fig. 10. Effect of different scavengers on the degradation of Rhodamine B dye in presence of catalyst. (a) C/C_0 Vs. Time plot and (b) percentage of dye degradation in presence of scavengers.

Experiments were carried out individually in presence of 1mM of isopropyl alcohol, EDTA and benzoquinone in the reaction mixture. All the scavengers were dissolved in Rhodamine B dye solution in presence of the catalyst and then photocatalytic activity of the samples was examined. In the presence of EDTA, the degradation rate of dye decreases drastically which proves that the holes generated during the photocatalytic reaction are scavenged, thereby inhibiting the catalytic reaction. With benzoquinone (in

presence of catalyst) also, a decrease in the rate of reaction is observed which suggests that the superoxide radicals are important in the catalytic reaction mechanism. Similarly the degradation rate was affected when isopropyl alcohol was added to the reaction mixture confining the role of hydroxyl studies. The above studies supports the mechanism of dye degradation as depicted in the schematic diagram (Fig. 9).

Conclusions

Delayed recombination of photogenerated excitons in Ag_3PO_4 occurs in presence of porous, Lewis acidic SiO_2 spheres. This has a strong impact on the photocatalytic dye degradation. The composite shows ~ 52 times enhancement in its efficiency as a photocatalyst with respect to pure Ag_3PO_4. The amount of SiO_2 played an important role in the composite for photocatalytic applications. The photodegradation rate increases upto a particular concentration of silver phosphate (0.26 min^{-1}) in the composite as compared to pure silver phosphate (0.005 min^{-1}). Being environment friendly, low cost silica nanoparticles is a promising support for composite materials to enhance the photocatalytic activity.

Acknowledgements

AKG thanks Department of Science & Technology (Nanomission), Department of Electronics and Information Technology (DeitY) and CSIR, Govt. of India for financial support. MS thank CSIR for the fellowship. KO thanks UGC, Govt. of India for the fellowship.

References

1. S. Zhang, H. Tian, S. Zhang, X. Wu, L. Song, J. Ye and Q. Wei, *J. Am. Ceram. Soc.*, 2013, **96**, 3536.
2. Q. Liang, W. Ma, Y. Shi, Z. Li and X. Yang, *CrystEngComm*, 2012, **14**, 2966.
3. H. Tong, S. Ouyang, Y. Bi, N. Umezawa Oshikiri and M. Ye, *J. Adv. Mater.*, 2012, **24**, 229.
4. J. Wang, J. Liu, C. Luo, Y. Lu and X. Yang, *Cryst. Growth Des.*, 2013, **13**, 4837.
5. Y. Bi, S. Ouyang, N. Umezawa, J. Cao and J. Ye, *J. Am. Chem. Soc.*, 2011, **133**, 6490.
6. M. Antonietti, B. Berton, C. Göltner and H. P. Hentze, *Adv. Mater.*, 1998, **10**, 154.
7. S. Mecking and R.Thomann, *Adv Mater.,* 2000, **12**, 953.
8. F. Honda, H. Honda, M. Koishi and T. Matsuno, *J. Chromatogr. A*, 1997, **775**, 13.
9. H. Wang, L. He, L. Wang, P. Hu, L. Guo, X. Han and J. Li, *CrystEngComm*, 2012, **14**, 8342.
10. O. D. Velev, K. Furusawa and K. Nagayama, *Langmuir* 1996, **12**, 2374.
11. Xu, X. Friedman, G. Humfeld, K. D. Majetich and S. A. Asher, *Chem. Mater*. 2002, **14**, 1249.
12. E. Petrovicova, R. Knight, L. S. Schadler and T. E.Twardowski, *J. Appl. Polym. Sci*., 2000, **77**, 1684.
13. Z. Yi, J. Ye, N. Kikugawa, T. Kako, S. Ouyang, H. Stuart-Williams, H. Yang, J. Cao, W. Luo, Z. Li, Y. Liu and R. L. Withers, *Nature. Mater.*, 2010, **9**, 559.
14. Y. Bi, S. Ouyang, J. Cao and J. Ye, Phys. *Chem. Chem. Phys.*, 2011, **13**, 10071.
15. W. Yao, B. Zhang, C. Huang, C. Ma, X. Song and Q. Xu, *J. Mater. Chem*., 2012, **22**, 4050.

16. G. Li and L. Mao, *RSC Adv*., 2012, **2**, 5108.

17. L. Zhang, H. Zhang, H. Huang, Y. Liu and Z. Kang, *New J. Chem*., 2012, **36**, 1541.

18. Z. M. Yang, G. F. Huang, W. Q. Huang, J. M. Wei, X. G. Yan, Y. Y. Liu, C. Jiao, Z. Wan, and A. Pan, *J. Mater. Chem. A*, 2014, **2**, 1750.

19. S. Kumar, T. Surendar, A. Baruah and V. Shanker, *J. Mater. Chem. A*, 2013, **1**, 5333.

20. X. Yang, H. Tang, J. Xu, M. Antonietti and M. Shalom, *ChemSusChem,* 2015, **8**, 1350.

21. W. Teng, X. Li, Q. Zhao and G. Chen, *J. Mater. Chem. A*, 2013, **1**, 9060.

22. J. Guo, S. Ouyang, H. Zhou, T. Kako and J.Ye, *J. Phys. Chem. C*, 2013, **117**, 17716.

23. J. Ren and H. Eckert, *J. Phys. Chem. C*, 2013, **117**, 24746.

24. W. Zhai, G. Li, P. Yu, L. Yang and L. Mao, *J. Phys. Chem. C*, 2013, **117**, 15183.

25. L. Liu, J. Liu and D. D. Sun, *Catal. Sci. Technol*., 2012, **2**, 2525.

26. X. Yang, H. Cui, Y. Li, J. Qin, R. Zhang and H. Tang, *ACS Catal.* 2013, **3**, 363.

27. H. Cuia, X. Yang, Q. Gao, H. Liu, Y. Li, H. Tang, R. Zhang, J. Qin, X. Yan, Mater Letters, 2013, **93**, 28.

28. X. Yang, J. Qin, Y. Jiang, K. Chen, X. Yan, D. Zhang, R. Li, H. Tang, *Appl. Catal. B,* Environmental, 2015, **166,** 231.

29. X. Yang, J. Qin, Y. Jiang, R. Li, Y. Li and H. Tang, *RSC Adv.,* 2014, **4**, 18627.

30. Y. Bi, H. Hu, Z. Jiao, H. Yu, G. Lu and J. Ye, *Phys. Chem. Chem. Phys.*, 2012, **14**, 14486.

31. C. T. Dinh, T. D. Nguyen, F. Kleitz and T. O. Do, *Chem. Commun*., 2011, **47**, 7797.

32. H. Li, S.Yin, Y. Wang, T. Sekino, S. W. Lee and T. Sato, *J. Mater. Chem. A*, 2013, **1**, 1123.

33. Y. G. Lin, Y. K. Hsu, Y. C. Chen, S. B. Wang, J. T. Miller, L. C. Chen and K. H. Chen, *Energy Environ. Sci.,* 2012, **5**, 8917.

34. J. K. Liu, C. X. Luo, J. D. Wang, X. H. Yang and X. H. Zhong, *CrystEngComm*, 2012, **14**, 8714.

35. T. Yan, W. Guan, W. Li and J. You, *RSC Adv.,* 2014, **4**, 37095.

36. M. Sharma, D. Das, A. Baruah, A. Jain and A. K. Ganguli, *Langmuir,* 2014, **30**, 3199.

37. A. Ganguly, T. Ahmad and A. K. Ganguli, *Langmuir*, 2010, **26**, 14901.

38. Y. Lei, L. D. Zhang, G. W. Meng, G. H. Li, X. Y. Zhang, C. H. Liang, W. Chen and S. X. Wang, *Appl. Phys. Lett*., 2001, **78**, 1125.

39. B. Xin, L. Jing, Z. Ren, B. Wang and H. Fu, *J. Phys. Chem. B*, 2005, **109**, 2805.

40. N. Ndiege, R. Chandrasekharan, A. D. Radadia, W. Harris, E. Mintz, R. I. Masel and M. A. Shannon, *Chem. Eur. J.* 2011, **17**, 7685 – 7693.

41. Y. Luan, Y. Feng, H. Cui, Y. Cao and L. Jing, *chempluschem*, 2014, **79**, 1271.

42. M. Shalom, S. Inal, D. Neher and M. Antonietti, *Catal. Today*, 2014, **225**, 185.

43. J. Mu, C. Shao, Z. Guo, Z. Zhang, M. Zhang, P. Zhang, B. Chen and Y. Liu, *ACS Appl. Mater. Interfaces*, 2011, **3**, 590.

Table of Content:

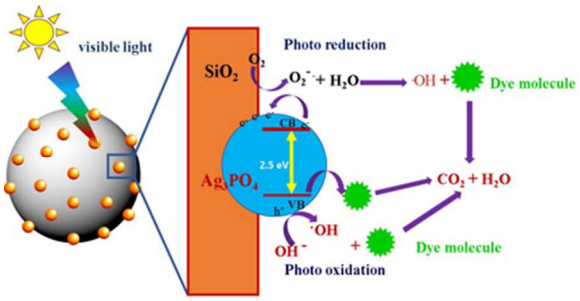

Light irradiation on Ag_3PO_4 decorated SiO_2 generates three reactive species (•OH, $O_2^{-\bullet}$, hole) leading to efficient photocatalysis.